Available online at www.sciencedirect.com
ScienceDirect
Journal of Sound and Vibration 307 (2007) 680–697
JOURNAL OF SOUND AND VIBRATION
www.elsevier.com/locate/jsvi

Parameter estimation and investigation of a bolted joint model

O.V. Shiryayev[a,*], S.M. Page[a], C.L. Pettit[b], J.C. Slater[a]

[a]*Department of Mechanical and Materials Engineering, Wright State University, 3640 Colonel Glenn Hwy., Dayton, OH 45435, USA*
[b]*Aerospace Engineering Department, United States Naval Academy, Annapolis, MA 21402, USA*

Received 10 June 2005; received in revised form 28 December 2006; accepted 27 June 2007
Available online 27 August 2007

Abstract

Mechanical joints are a primary source of variability in the dynamics of built-up structures. Physical phenomena in the joint are quite complex and therefore too impractical to model at the micro-scale. This motivates the development of lumped parameter joint models with discrete interfaces so that they can be easily implemented in finite element codes. Among the most important considerations in choosing a model for dynamically excited systems is its ability to model energy dissipation. This translates into the need for accurate and reliable methods to measure model parameters and estimate their inherent variability from experiments. The adjusted Iwan model was identified as a promising candidate for representing joint dynamics. Recent research focused on this model has exclusively employed impulse excitation in conjunction with neural networks to identify the model parameters. This paper presents an investigation of an alternative parameter estimation approach for the adjusted Iwan model, which employs data from oscillatory forcing. This approach is shown to produce parameter estimates with precision similar to the impulse excitation method for a range of model parameters.
Published by Elsevier Ltd.

1. Introduction

Built-up structures are commonly assembled by joining their components through bolted or riveted connections. In recent decades, the design process for complex structures has become largely reliant on numerical analysis and simulations. Efforts to improve the predictive power of these models have generated widespread interest in faithfully representing the dynamics of mechanical joints. The primary impediments to modeling mechanical joints are their nonlinear nature and variability. Variability arises from inconsistencies in their assembly as well as from a number of age-related factors, including fatigue, relaxation, corrosion, and maintenance.

The primary effect of bolted and other mechanical joints on the dynamics of structures is that they are significant sources of damping. Ibrahim and Pettit [1] cite a number of energy dissipation processes, including friction in the screw-nut thread interface, gas pumping induced by local micro-gaps between joint surfaces, material damping, and plastic deformation in the asperities of contact surfaces. Furthermore, the net stiffness

*Corresponding author. Tel.: +1 937 775 5040; fax: +1 937 775 5009.
E-mail address: shiryayev.2@wright.edu (O.V. Shiryayev).

0022-460X/$ - see front matter Published by Elsevier Ltd.
doi:10.1016/j.jsv.2007.06.033

of the joint is affected not only by the elastic properties of the joint's materials but also by the hardness and roughness of the contact surfaces.

These properties are extremely difficult to model in detail and can vary substantially both during the life of a given joint (e.g., through relaxation) and from one joint to another under nominally similar assembly processes and environmental conditions. Although some sophisticated finite element software packages allow modeling of the complex physics at the joint interface, it is neither practical nor necessary to apply this micro-scale approach to models of large structures such as airframes. Sufficient increases in predictive power beyond common practice should be available through macro-scale or phenomenological joint models. These models must satisfy several conflicting goals; in particular, they should provide a good compromise between accuracy, adaptability, ease of implementation, and ease of identification. Joint models also should offer features that will allow them to become integral components of risk estimation for the assembled system. This is becoming increasingly important as individual industries continue their extended transitions toward risk-based or risk-informed design. Joint models therefore should reflect the uncertainty in joint properties and depend on parameters that are readily identified from experimental data. These considerations show that the focus of research in this area should be on developing compact joint models that accurately and efficiently represent the dynamic properties and their variability when they are included in large models of built-up structures.

A number of bolted joint models are documented in the literature. Brief overviews of several existing macro-scale models are given by Yue [2] and Pettit et al. [3]. Joint models can generally be categorized as either: (i) physics-based, (ii) experiment-based (which are sometimes known as model-free methods), or (iii) joint parameter identification-based substructuring methods [2]. The first two classes focus on the properties and behavior of the joint; the third class depends on how the insertion of a joint alters the response of connected substructures. The third approach is also complementary to the physics-based and experiment-based methods in that it offers an alternative path for identifying the model's relevant parameters. This path was followed by Yue [2] in a recent thesis.

A prominent research direction employs recently developed extensions of Iwan elements [4,5], which involve parallel combinations of spring-slider (i.e., Jenkins) elements to represent hysteresis in bolted joints. In order to assess the ability of the model to capture natural variability of the joint, it is necessary to develop a reliable and accurate parameter identification method in parallel with detailed laboratory experiments. Recent studies have emphasized using impulse excitations to identify the model parameters [3,5]. Herein we describe a method for parameter estimation that employs oscillatory forcing and compare it with impulse excitation results.

We have endeavored to develop an alternate means of identifying the joint parameters for two related reasons: (i) model-based risk prediction requires that sufficient information be available to assess the dependability of the response predictions and (ii) because the model is inherently nonlinear, the uniqueness of the impulse-identified model parameters is in question. The first reason is a direct consequence of the general desire to obtain evidence that either corroborates or disputes the accuracy of a given model. In response to this concern, we decided to pursue sinusoidal excitation because it is in some sense an orthogonal approach to impulse excitation and because it is expected that these models would be employed in simulating response to continuous excitations, not impulse loads. The second concern reflects that adequate performance of nonlinear dissipation elements must include the ability to exhibit hysteresis similar to the actual joint. There is some concern that impulse excitation will not generate a sufficiently wide range of behavior to identify parameters that are appropriate for modeling the response due to general types of continuous excitation.

2. Adjusted Iwan model and parameter estimation methods

2.1. Adjusted Iwan model

Iwan [6,7] developed an elasto-plastic model that can be used to account for the nonlinear stiffness and energy dissipation at the joint interface. His model is composed of a parallel system of spring-slider elements, which are also known as Jenkins elements, as shown in Fig. 1(a). The strength of a Jenkins element is the applied force it can support with slipping, which is the maximum friction force that can be generated by its

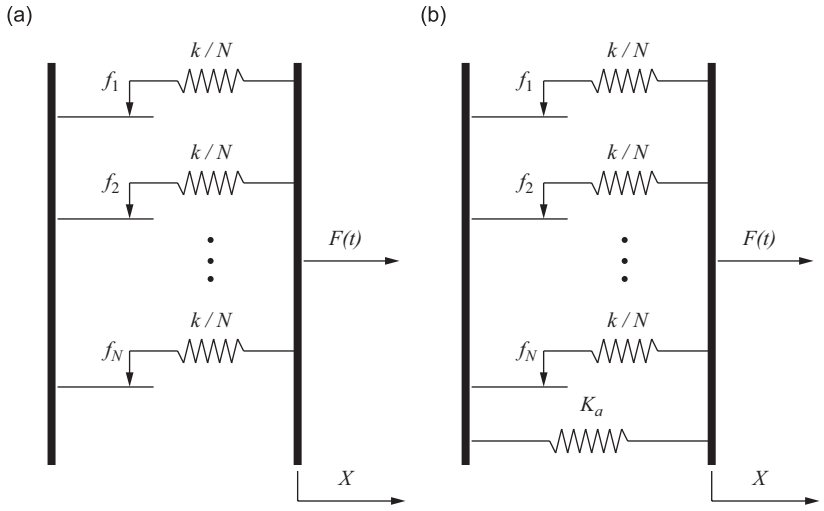

Fig. 1. Iwan hysteretic models: (a) original Iwan spring-slider model; (b) adjusted Iwan model.

slider. The full joint's slip force is assumed to be the average slip force of the population of sliders. Micro-slip denotes a state in which the applied force causes a minority of the sliders to slip but the joint's slip force has not been exceeded. Macro-slip is in essence a limiting case of micro-slip, which exists for applied forces greater than the slip force of the full joint.

Segalman [4] applied Iwan's model to describe the behavior of lap-type joints under the axial harmonic loads. The force–deflection curve defined by the model is governed by the distribution of the sliders' yield or slip forces. Segalman assumed that the joint possesses zero stiffness after the macro-slip occurs, and considered the density function to be a sum of the truncated power law distribution and the Dirac delta function:

$$\rho(\sigma) = R\sigma^{\chi}[U(\sigma) - U(\sigma - \sigma_{\max})] + \mathscr{Y}\delta(\sigma - \sigma_{\max}). \tag{1}$$

In Eq. (1), U is the Heaviside step function, and $\sigma_{\max}$ is the upper limit of the distribution function. Four parameters are needed to uniquely define the model: χ, $\sigma_{\max}$, f_y, and $\beta = \mathscr{Y}/(R\sigma_{\max}^{\chi+1}/(\chi+1))$. The slip force of the joint, f_y, is obtained directly from force–deflection measurement data, while χ and β are calculated by curve-fitting the experimentally obtained cyclic energy dissipation in the joint versus the applied load. The fourth parameter, $\sigma_{\max}$, is calculated using the equations that relate the displacement amplitude of harmonic motion to the cyclic energy dissipation and the first three parameters. Segalman's report [4] demonstrates the capability of this formulation of Iwan's model to capture cyclic energy dissipation under harmonic loads.

Song et al. [5] developed a slightly different type of Iwan model, which they called the adjusted Iwan model. This enhancement of the Iwan model takes into account the experimental fact that a joint retains a small stiffness when macro-slip occurs, i.e., when all of the Jenkins elements slip. The adjusted Iwan model is produced by adding a spring in parallel with the Jenkins elements, as depicted in Fig. 1(b).

Song also introduced the adjusted Iwan beam (AIB) element. This two-dimensional element employs two adjusted Iwan models, assembled to account for the relative transverse displacement and rotation between the nodes. Its formulation and coupling with standard beam finite element models is presented below, but first the identification of adjusted Iwan element parameters is discussed.

2.2. Parameter estimation methods

In order to create a faithful finite element model of a particular joined structure with AIB elements, the parameters of the two adjusted Iwan models must be identified from the measured response data. Six parameters must be determined for each element, i.e., three for each adjusted Iwan model. The parameter $\alpha_i = k/k_a$ represents the ratio between the stiffness before and after macro-slip occurs, and f_{y_i} $(i = \{1, 2\})$ is

the force level at which macro-slip occurs. The distribution density function is assumed to be uniform, with width Δ_i and mean f_{y_i}. The third parameter therefore is defined as

$$\beta_i = \frac{\Delta_i}{2f_{y_i}}. \tag{2}$$

Since some micro-slip can be observed even at very small loads, it is assumed that $\Delta_i = 2f_{y_i}$, or $\beta_i = 1$; therefore, only two parameters for each adjusted Iwan model are independent. In order to simplify the identification procedure, it is assumed that both Iwan models in the AIB elements have the same parameters, $\alpha_1 = \alpha_2$ and $f_{y_1} = f_{y_2}$. Relaxing this constraint might provide better fits to measured data, but also would increase the propensity to overfit. The above assumptions were utilized in previously published work [3,5], where it was found to produce a fairly dependable representation of joint dynamics under impulse excitation. Their suitability for more general excitation is not clear yet.

2.2.1. Estimation on the impulse response data

Parameter estimation for nonlinear systems is generally difficult. The hysteretic behavior of the AIB element dictated by the adjusted Iwan models must account for a majority of the energy dissipation in the structure under consideration. Hence, it is reasonable to conclude that in order to estimate parameters for the two adjusted Iwan models, one needs to consider measurement data that contains information about energy dissipation in the system. Song et al. [5] decided to utilize decay envelopes of the impulse response for parameter estimation.

Owing to their powerful mapping capabilities, neural networks are employed for parameter estimation. Neural networks have been widely used for parameter estimation in various fields because they are readily trained to learn complex relationships between input and output data and they offer the ability to be regularized so as to avoid overfitting small-scale components (e.g., noise) in the training data. These capabilities make them useful for solving inverse problems like those encountered in identifying nonlinear systems. The neural network based identification procedure developed by Song et al. [5] is outlined below.

(1) The joined structure is excited by the impact hammer. The input (hammer force) and acceleration (response) time histories are recorded.
(2) For each combination of α_i and f_{y_i} from a set of AIB element parameters, the response of the finite element model to the measured forcing is calculated.
(3) Decay envelopes are computed from the simulated and measured response data.
(4) A neural network is built and trained to match the decay envelopes from simulated data. The neural network accepts as input a decay envelope and maps the envelope to a corresponding set of AIB element parameters.
(5) AIB element parameters of the actual structure are estimated by feeding the measured envelope into the trained neural network.

The above identification method appeared to work relatively well, allowing the finite element model to replicate the response of the structure, at least in a global manner. An important component of the method is the way in which the envelopes are estimated from the decay time histories. Both measured and simulated data contain high-frequency transients due to higher modes; hence Hartwigsen et al. [8] filtered the data and then applied the Hilbert transform to obtain the envelope. In their slightly earlier publication dealing with AIB element parameter estimation, Song et al. [5] did not provide a thorough description of their envelope estimation procedure method. It was mentioned that in order to obtain the training data for the network, the envelope was fitted with a polynomial, which was then evaluated at prescribed time points. The data sets obtained from all envelopes was then regularized and used for training the neural network.

Pettit et al. [3] used a different approach to obtain training data. Local maxima points were found in the time history by tracking the changes in the sign of the forward difference of the time history. To minimize the inclusion of maxima due to high-frequency transients, the entire time history was divided into a number of intervals. Then on each interval, a point with highest magnitude was found. The length of each interval was obtained as $t_{\text{int}} = 1/f_{\max}$, where $f_{\max}$ is the point with maximum magnitude of the power spectrum density of

the signal. The decay envelope was obtained by fitting cubic splines between successive maxima points. The splines were then evaluated at prescribed time points to produce the data for training the neural network. Although the method described above is not fully immune to detrimental effects of high-frequency transients, the estimated AIB element parameters resulted in relatively accurate representation of the dynamics of the joined structure.

2.2.2. Estimation on the oscillatory forcing data

In this approach, response data from single frequency sinusoidal bending excitation is considered. This form of forcing can be easily implemented on the laboratory specimen and simulated numerically. Estimation problems require data that contain enough features to describe a system's behavior throughout a reasonable range of realizations of the system parameters. Steady-state vibration data are not as descriptive of a joint's dissipative effects as free decay data. However, from numerical simulations and experimental measurements it was observed that oscillatory time histories contain certain features that can be exploited for parameter estimation.

In this work, the wavelet transform is utilized to describe the features of the signal that can be used for identification. The continuous wavelet transform represents a signal as a sum of scaled and shifted wavelets, which are localized in time and oscillatory, so that they have zero mean. Wavelet analysis reveals local or scale-dependent features, such as discontinuities in a process or its derivatives as well as self-similar (fractal) features. In signal processing, it offers a perspective that is complementary to conventional Fourier analysis, which decomposes a signal into its constituent frequencies and their respective phases. Fourier analysis hides local signal features in the strength of each frequency component along with the relative phases. Wavelet analysis naturally uncovers the location and extent of a particular events in a signal. Hence, the wavelet transform involves the time-scale domain rather the frequency domain of the Fourier transform and the time-frequency domain of the windowed or short-time Fourier transform. The scale and mean frequency of a wavelet are inversely related because scaling the wavelet involves stretching or compressing its support, but the relationship is only approximate because wavelets are oscillatory but not truly periodic.

A continuous wavelet transform results in a matrix of wavelet coefficients, which vary by scale and position. It was decided that the mapping of the wavelet coefficients and adjusted Iwan element parameters be provided by the use of neural networks. To allow for better (easier) distinction between the various realizations of the model parameters, strain measurements were used in the identification process. The general identification procedure that employs oscillatory data involves the steps described here. Specific implementation details will be cited at appropriate places in later sections.

(1) The joined structure is excited in bending with a sinusoidal input. The manner in which this is performed is described in Section 3. Acceleration and strain outputs are recorded along with the frequency and amplitude of the input.
(2) For each combination of α and f_{yi} from a range of AIB element parameters, the steady-state response of the finite element model (see Section 4) is obtained for a bending input with the same frequency and amplitude as in the experimental case.
(3) A continuous wavelet transform is applied to acceleration and strain data. The scale of wavelet coefficients of interest is chosen to be representative of prominent features in the steady-state signal that appear to result from nonlinearity in the joint.
(4) Principal component analysis is applied to the wavelet coefficient data obtained from all computational realizations of AIB element parameters. This allows for compact representation of the data, which reduces computational requirements and improves the robustness of the neural network-based identification procedure.
(5) A neural network is trained to map the principal component coefficients in the wavelet transform of the finite element model output to the known AIB element parameters, α and f_{yi}.
(6) AIB element parameters of the actual structure are obtained by feeding the principal component coefficients calculated from the corresponding scale of the wavelet transform of the measured data into the network.

Previous work by Song et al. [5] considered only the response of the structure due to impulsive loads. Our literature search revealed no previous attempts to investigate the ability of the AIB element to represent the

steady-state dynamics due to oscillatory bending excitation. The objective of this paper is to apply the AIB element to model a bolted joint under steady-state oscillatory forcing, and thereby investigate the use of an alternative parameter estimation method for comparison with impulse-estimated AIB element parameters. In doing so, we attempt to investigate whether a unique set of parameters chosen through a particular identification procedure is able to represent the dynamics of the joined structure subjected to different types of excitation.

3. Experiments

The experimental specimen is similar to a double lap joint but with only a single bolt (see Fig. 2), which is instrumented for load measurements. The slot in the joint was generated by wire electrical discharge machining, and is extended to allow sufficient flexibility for good surface contact between the inner normal surfaces. The large compliance also ensures that the normal load measured in the instrumented bolt is very close to the load of all contact surfaces. The joint is designed so that contact occurs at horizontal interfaces adjacent to the bolt. The specimen and bolt are made of 7075 Al. Two large masses are integrally constructed at the ends of the joined beams. These masses are used to reduce the extensional natural frequency of the beams. The design results in well-isolated modes in bending and extension. The specimen is supported by 0.01 in. (0.254 mm) diameter stainless steel wire attached at the nodes of the first bending mode. This support method approximates free–free boundary conditions. The wire is sufficiently long to reduce the pendulum frequency to approximately 0.5 Hz, which is far below the modal frequencies of the joined beam.

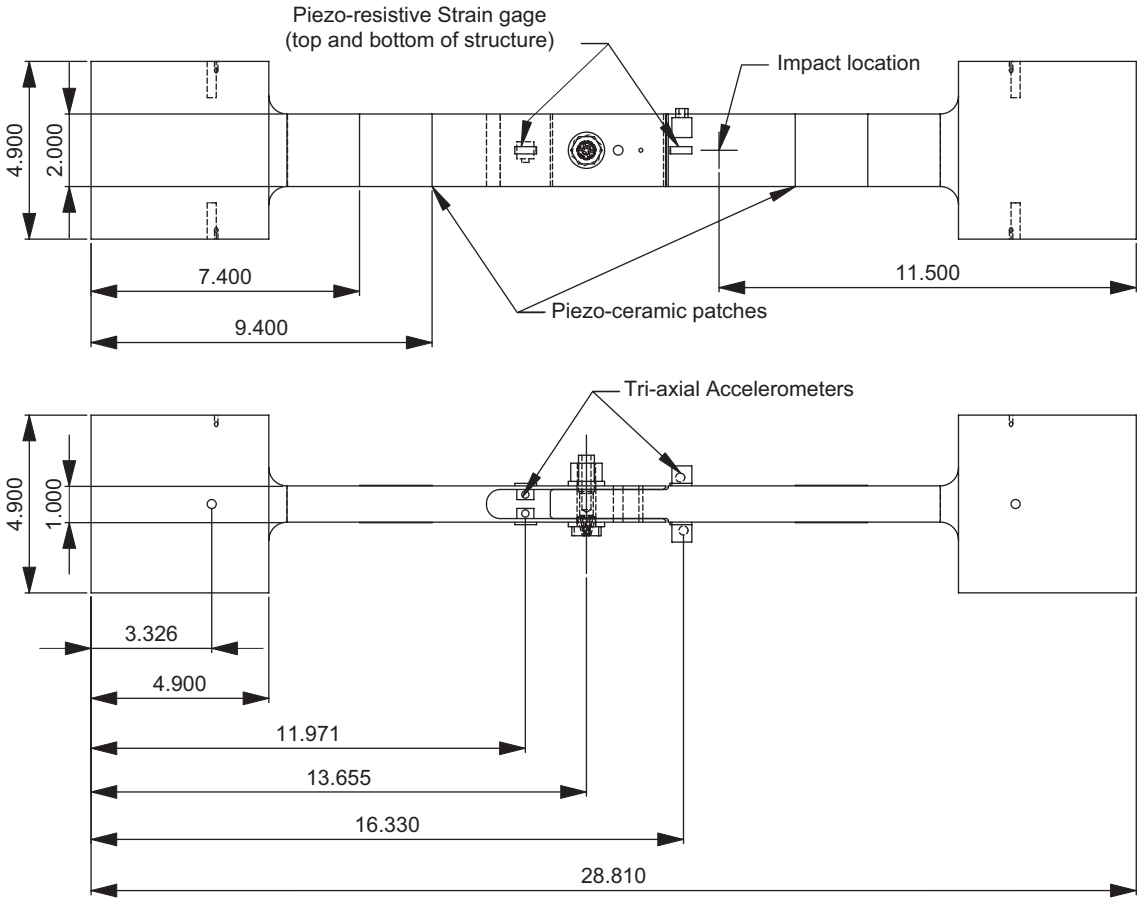

Fig. 2. Dimensions of lap joint experiment and instrumentation locations (dimensions in inches).

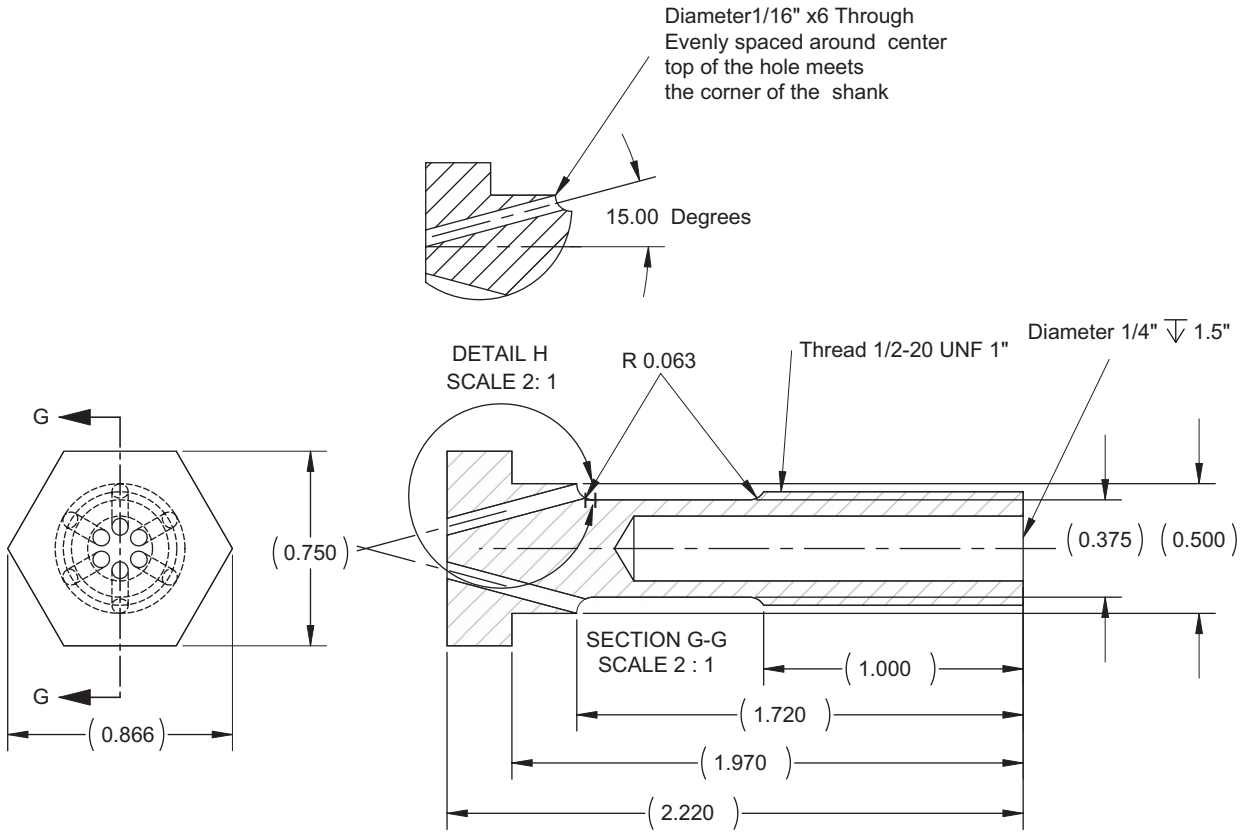

Fig. 3. Instrumented bolt drawing.

Three forms of excitation are used. Forced response is performed using piezo-ceramic patches located symmetrically on the test article, impulse response is generated with an impact hammer, and an electrodynamic shaker is used for large amplitude transverse bending excitation. Instrumentation includes piezo-resistive strain gages and tri-axial accelerometers next to the bolt (see Fig. 2). Having these sensors allows for measuring the response of the structure from both sides of the joint for hysteresis plots. The piezo-ceramic patches are wired to allow bending and extensional excitation, but only bending was employed to generate the results presented herein. The bolt (Fig. 3) is instrumented with four strain gauges to measure tensile load, torque, and bending of the bolt during the experiment. Force input into the structure by the shaker is measured via a PCB 708 A50 force transducer.

4. Computational modeling of the joined specimen

An initial numerical model of the experiment was created in ABAQUS [9] with B21 beam elements, which employ the Timoshenko formulation. However, owing to the complexity of defining custom elements in ABAQUS, it was decided that implementation of the AIB element would be facilitated by importing element matrices from ABAQUS into MATLAB [10] where they were reassembled. The joined specimen was then modeled in MATLAB by using the AIB element to generate appropriate internal force vectors at the nodes of this element. The equations of motion for the joined beam can be written as

$$(\mathbf{M}^{\text{elastic}} + \mathbf{M}^{\text{AIBE}})\ddot{\mathbf{x}} + \mathbf{C}\dot{\mathbf{x}} + \mathbf{K}^{\text{elastic}}\mathbf{x} + \mathbf{F}_{\text{AIBE}}(\mathbf{x}) = \mathbf{F}_{\text{ext}}, \tag{3}$$

where $\mathbf{M}^{\text{elastic}}$ and $\mathbf{M}^{\text{AIBE}}$ are portions of the global mass matrix that correspond to the linear elastic elements and AIB element, respectively. $\{\mathbf{K}^{\text{elastic}}\mathbf{x}\}$ is the vector of nodal forces due to linear elastic elements and $\{\mathbf{F}_{\text{AIBE}}(\mathbf{x})\}$ is the vector of nodal forces due to the AIB element.

Modal analysis of the surrogate monolithic beam was performed to estimate the material damping in the joined beam. A viscous damping matrix **C** was constructed using the damping ratios identified from the measurements of the monolithic specimen. Table 1 contains the data for bending modes obtained during the test and the corresponding natural frequencies calculated from the finite element model. For modal calculations a linear B21 element was used in place of the nonlinear AIB element.

The computed natural frequencies for the first and second modes are very close to the measured values. The natural frequencies for the third and fourth mode in the finite element model are significantly higher than the measured values. This is largely due to the way the boundary conditions were applied in the model. Owing to numerical difficulties that arose in modeling the cable supports, it was chosen to fix vertical displacement in the model at the nodes that are very close to the actual nodal points of the first bending mode of the beam. However, the actual nodal locations for the third and fourth modes are spread out further towards the ends of the beam, compared to the nodal points of the first and second mode. The artificial constraint stiffens the system and hence increases the corresponding natural frequencies.

Better correspondence between the finite element model and the true system would of course be preferred when performing parameter estimation through comparison of measured data with predictions. Estimation technique based on the decay envelopes is concerned with the large-scale response features, so the higher modes should not seriously alter the decay or the resulting identified parameters. The features that were used for parameter identification from oscillatory data were based on the harmonics that were at the multiples of the excitation frequency. Hence, in this work a perfect match between the finite element model and the experiment appeared not to be crucial.

Table 1
Modal parameters of the monolithic beam

	Mode			
	1st	2nd	3rd	4th
Measured natural frequency, Hz	126.9	321.9	716.9	1473.1
Calculated natural frequency, Hz	125.2	329.1	814.2	1696.0
% Error	−1.33	2.24	13.57	15.13
Modal damping ratio ξ, %	0.06	0.03	0.04	0.04

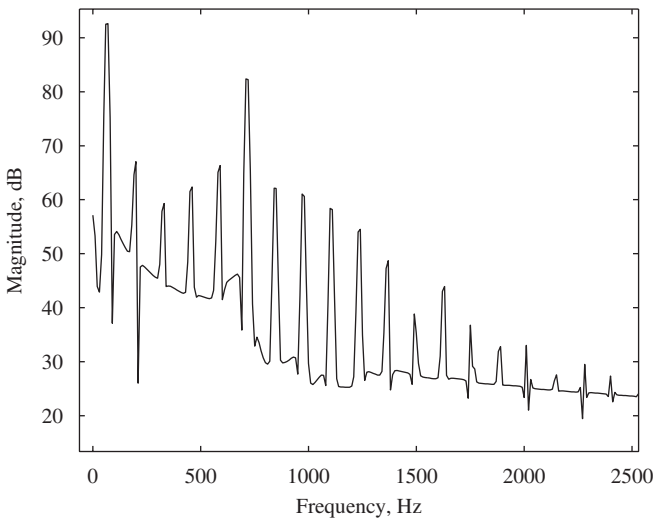

Fig. 4. Acceleration response spectrum.

Since the problem is nonlinear, an explicit central difference method was employed for time integration [11]. This algorithm is conditionally stable; i.e., the time step has to be smaller than a certain critical value to be able to obtain a stable solution. This was not a limitation in the current solution because a relatively small time step was required to maintain accuracy (Fig. 4).

5. Results

5.1. Estimation from decay envelopes

It was decided to first obtain some baseline estimation results by replicating the work done by Song et al. and estimating the AIB element parameters based on the decay envelopes. The joined structure was excited with an impact hammer at a point to the left of joint, which corresponds to an element node in the finite element model. The response in the vertical direction on the other side of the joint was measured with an accelerometer. Due to the complexity of this estimation problem, it requires significant user intervention during the data processing and parameter estimation stages. User adjustments usually involve, but are not necessarily limited to choosing the number of time points in the envelope, architecture of the neural network and the choice of neuron transfer functions. The results presented herein and in Ref. [3] are based on different data and a different experiment, so the details of identification procedure described in this section are also somewhat different. In this work, described herein linear polynomials were fit between the maxima points found in the response. The polynomials were then evaluated at 30 prescribed points in time to produce the associated envelopes.

A multi-layer, feed-forward neural network was built in MATLAB to estimate the parameters for the AIB element. The network had a single hidden layer of 20 neurons and an output layer with two neurons for the slip force f_{yi} and stiffness ratio α. All neurons were defined to have a log-sigmoid transfer function [12],

$$\text{logsig}(x) = \frac{1}{1+e^{-x}}. \tag{4}$$

This function restricts the output to the interval $[0, 1]$, but this is not a limitation for obtaining f_{yi} because all inputs and outputs were normalized to improve training. The envelopes for the training data set were obtained from the numerically generated response for a range of AIB element parameters. The slip force f_{yi} was varied from 600 to 800 N with an increment of 20 N. The stiffness ratio α was varied from 0.4 to 0.8 with an increment of 0.1. Fig. 5 illustrates that the experimental envelope is within the region spanned by the envelopes obtained from numerical simulations.

The network was trained using an error back-propagation algorithm. The envelope obtained from an initial hammer test with a maximum impact force of approximately 130 N was fed into the network, which estimated the parameter values to be $f_{yi} = 649.3$ N, and $\alpha = 0.6382$. The response of the finite element model obtained with these values is compared to the measured acceleration in Figs. 6(c) and (d). The time histories are in good global agreement. Although some differences in the fine details are visible due to unmodeled dynamics of the apparatus. From Fig. 6(b) one can observe that the measured envelope displays some low-frequency oscillations, which are attributed to the structure vibrating on the steel support wires, but the envelope from simulated data passes between the peaks and valleys of the measured envelope because the model does not include the flexibility of the supports.

In order to further validate the estimated model parameters, two additional hammer tests were performed on the specimen. The force data measured during those tests were input into the finite element model and the acceleration time histories were generated. In the first case, the impulse magnitude was approximately 100 N, and in the second case the magnitude was near 166 N. Figs. 7 and 8 compare the measured and simulated time histories. The numerical results accurately simulate the decay in the experiment albeit in a smoothed manner. Hence, it can be stated the estimated set of AIB element parameters allows for reasonably accurate modeling of the response due to impact excitation. Note that the analytical estimate for the joint slip force (based on the clamping force in the joint) was found to be approximately 900 N. This value is much higher than the loads used in the experiment.

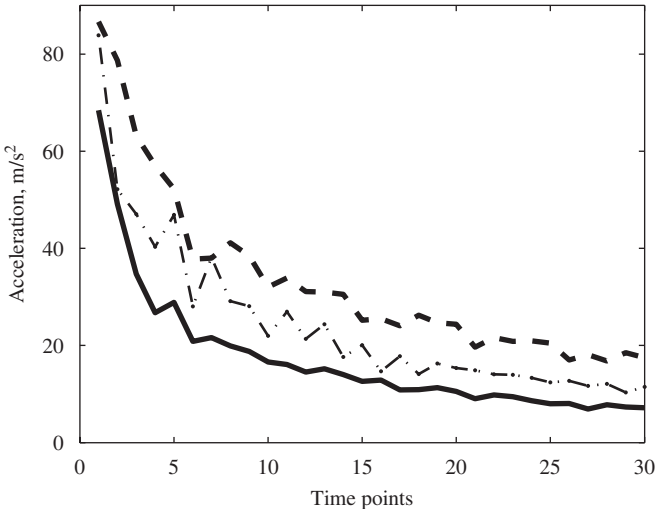

Fig. 5. Decay envelopes: —— high dissipation, - - - low dissipation, — · —· experimental.

5.2. Estimation from oscillatory data

In this work, the joined structure was excited in bending with oscillatory excitation at 65 Hz. This is significantly below the first resonant frequency, which allows observation of the features in the signal, i.e., additional harmonics, that are caused by the nonlinearity in the structure. In contrast, resonant excitation produces response in which the magnitude of the resonant mode is extremely large compared to that of the other modes. This makes it practically impossible to discern other harmonics in the signal.

An initial study showed that the amount of excitation that was provided by the PZT patches was insufficient to observe response features necessary for identification; hence, an electrodynamic shaker was selected to provide excitation. The shaker is attached to the location on the specimen that was used in the cases with impact hammer excitation as shown in Fig. 9. All possible effort was made to ensure that the shaker attachment did not exert measurable static force on the specimen, i.e. it would not act as an additional static support.

The steady-state response of the joined structure due to sinusoidal bending input was simulated by direct integration of the equations of motion. The excitation signal for numerical simulations was similar to the one recorded during the experiment, which represented a sinusoidal waveform with an amplitude of approximately 21.41 N. The response that was generated for the same set of AIB element parameters employed for the decay envelopes, $f_{yi} \in \{600, 620, \ldots, 800\}$ and $\alpha \in \{0.4, 0.5, \ldots, 0.8\}$, appeared to have much smaller amplitude than that observed in the experiment, so this became an important focus of the study.

Using parameters from the range estimated with the impulse response measurements, the simulated response from the model does not contain additional harmonics that are present in the measured signal. Simulations were run with several combinations of the AIB element parameters until it was found that results for $f_{yi} \in \{80, 100, \ldots, 220\}$ and $\alpha \in \{0.10, 0.15, \ldots, 0.30\}$ correlated better with the higher frequencies in the measured data. This parameter range suggests higher energy dissipation than was identified with the hammer excitation, which would appear to indicate a looser joint. However, the joint was torqued to nominally the same value before the hammer and forced oscillation tests. Moreover, the torque was checked after the oscillatory tests and found to have changed only slightly, so it is unlikely that the slip and dissipation would have changed substantially. Comparison of the hammer and forced oscillatory tests therefore indicates that a single set of parameters is not able to represent the response of the joint to a variety of forcing functions. In particular, AIB element parameters obtained with impact excitation might not be appropriate for simulating the response to extended dynamic excitation.

Fig. 10 shows two generated acceleration time histories plotted along with the measured one. The time history denoted *low dissipation* corresponds to higher f_{yi} and α from the range mentioned above, i.e.,

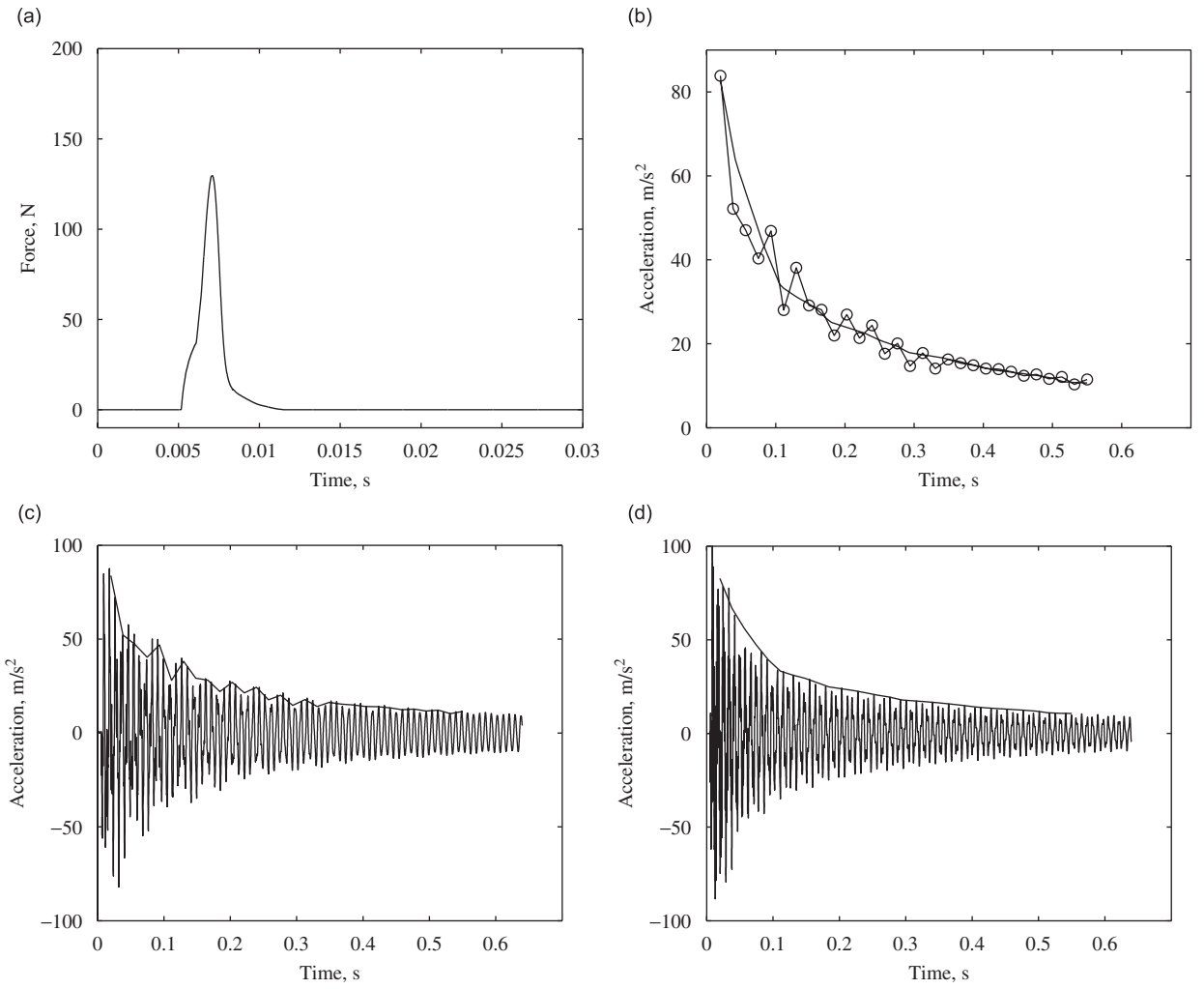

Fig. 6. Results for the case used for training, 130 N impact: (a) forcing signal; (b) experimental and simulated envelopes, — ○ — measured, ... simulated; (c) measured response; (d) simulated response.

$f_{yi} \in \{80, \ldots, 220\}$ and $\alpha \in \{0.10, \ldots, 0.30\}$. The data designated by *high dissipation* corresponds to lower values of f_{yi} and α in that range. The data designated *low dissipation* appears to have little presence of higher harmonics, while the data denoted *high dissipation* contains the presence of higher harmonics comparable to that in the measured data but its overall amplitude is large relative to the measured data. Hence, the selected parameter range for the training data was $f_{yi} \in \{80, 100, \ldots, 220\}$ and $\alpha \in \{0.10, 0.15, \ldots, 0.30\}$. A validation data set was also generated with the training range $f_{yi} \in \{90, 110, \ldots, 210\}$ and $\alpha \in \{0.12, 0.17, 0.22, 0.27\}$.

A continuous wavelet transform was applied to the obtained acceleration and strain time histories. It must be noted that the strain data was normalized to unity prior to any processing since calibration data was not available for the strain gages. The *Gaus2* wavelet was used in this work [13]. This wavelet belongs to the Gaussian derivatives family, and is based on the second derivative of the Gaussian probability density function. The scale of wavelet coefficients was picked visually so as to be representative of the features in the signals and hence improve the ability to distinguish between the various realizations of the AIB element parameters.

Principal component analysis was applied to reduce the amount of data needed for training the neural net and to improve the robustness of the identification procedure. Let $\mathbf{S}_{n\times m}$ be a matrix, where each column represents the wavelet coefficients for a single realization of AIB element parameters. Matrix $\mathbf{V}$ is formed as

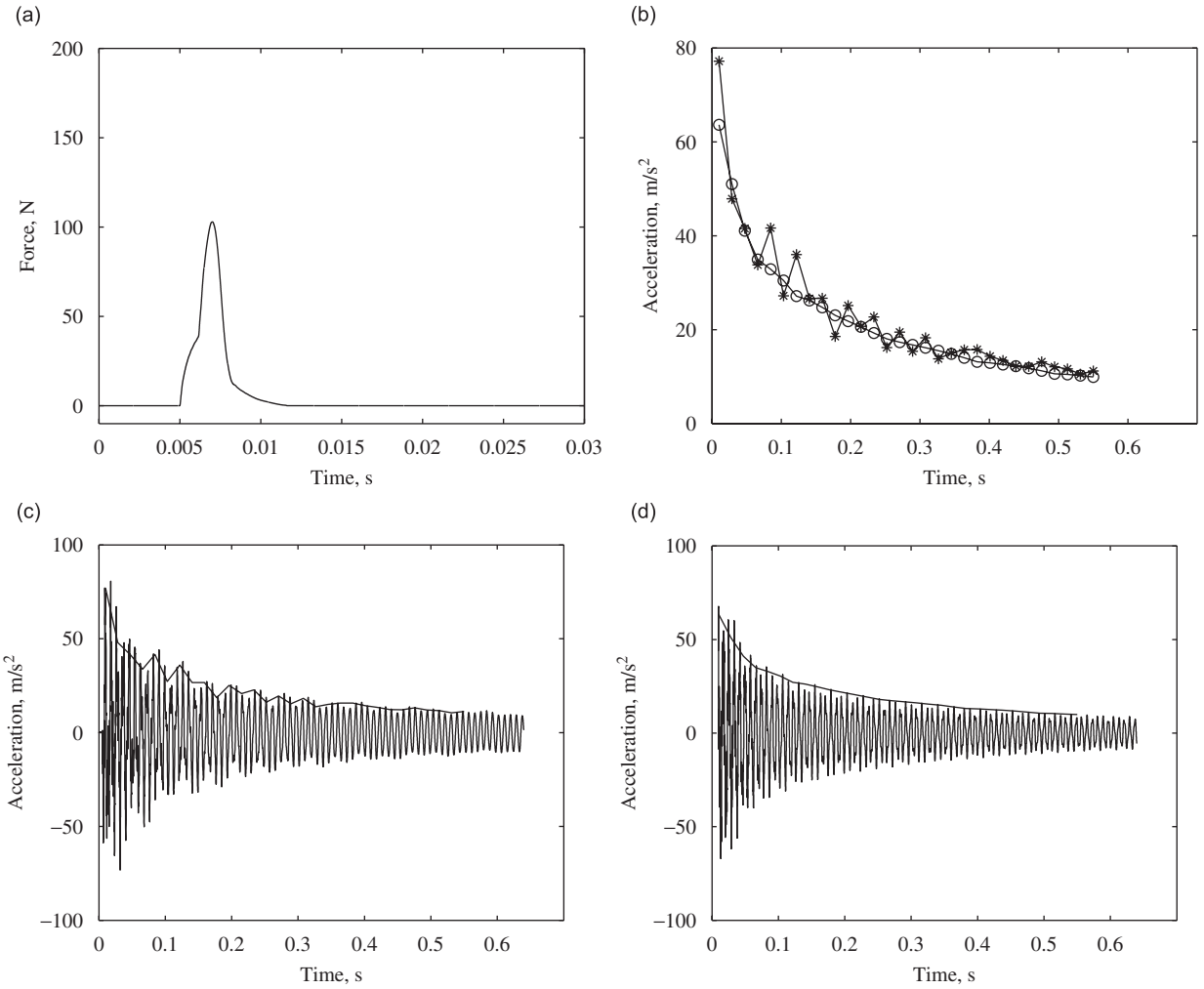

Fig. 7. Results for the validation case with 100 N impact: (a) forcing signal; (b) experimental and simulated envelopes, — ○ — measured, ... simulated; (c) measured response; (d) simulated response.

$\mathbf{V}_{m\times m} = \mathbf{S}^{\mathrm{T}}\mathbf{S}$. Principal components are obtained by solving the eigenvalue problem for the matrix $\mathbf{V}$. This results in the matrix of eigenvalues $\mathbf{\Lambda}_{m\times m}$ and a matrix of the corresponding eigenvectors $\mathbf{\Phi}_{m\times m}$. One assembles the matrix $\mathbf{\Phi}^{\mathbf{R}}_{m\times p}$ of p principal components that are desired to be retained based on the magnitudes of the corresponding eigenvalues. Then, the mapping matrix between the n-dimensional data space and the p-dimensional principal component space is obtained as $\mathbf{\Psi}_{n\times p} = \mathbf{S}\mathbf{\Phi}^{\mathbf{R}}$. The original wavelet coefficient data for the **i**th realization of parameters for AIB element can be represented in terms of the reduced-order mapping functions as $\mathbf{S}^{\mathbf{i}}_{n\times 1} = \mathbf{\Psi}_{n\times p}\mathbf{a}^{\mathbf{i}}_{p\times 1}$, where $\mathbf{a}^{\mathbf{i}}_{p\times 1}$ is a feature vector of regression coefficients for the **i**th parameter realization. Each vector $\mathbf{a}^{\mathbf{i}}$ is obtained by pseudo-inverse as $\mathbf{a}^{\mathbf{i}} = (\mathbf{\Psi}^{\mathrm{T}}\mathbf{\Psi})^{-1}\mathbf{\Psi}^{\mathrm{T}}\mathbf{S}^{\mathbf{i}}$.

Fig. 11 contains plots of the magnitudes of the eigenvalues obtained for acceleration and strain wavelet coefficient data. Four acceleration modes and 3 strain modes were kept as a result of minimal participation of higher modes. Each realization of parameters for the AIB element was thus represented in terms of a 4×1 coefficient vector for acceleration data and a 3×1 vector for strain data.

The multi-layer feed-forward neural network was built and trained on the reduced data. The network contained two input layers, the first containing 4 neurons to accept the data based on acceleration, and the second containing 3 neurons to accept the data based on strain. The network had 4 hidden layers of which the first two contained 36 neurons each, the third layer contained 30 neurons, while the last hidden layer contained

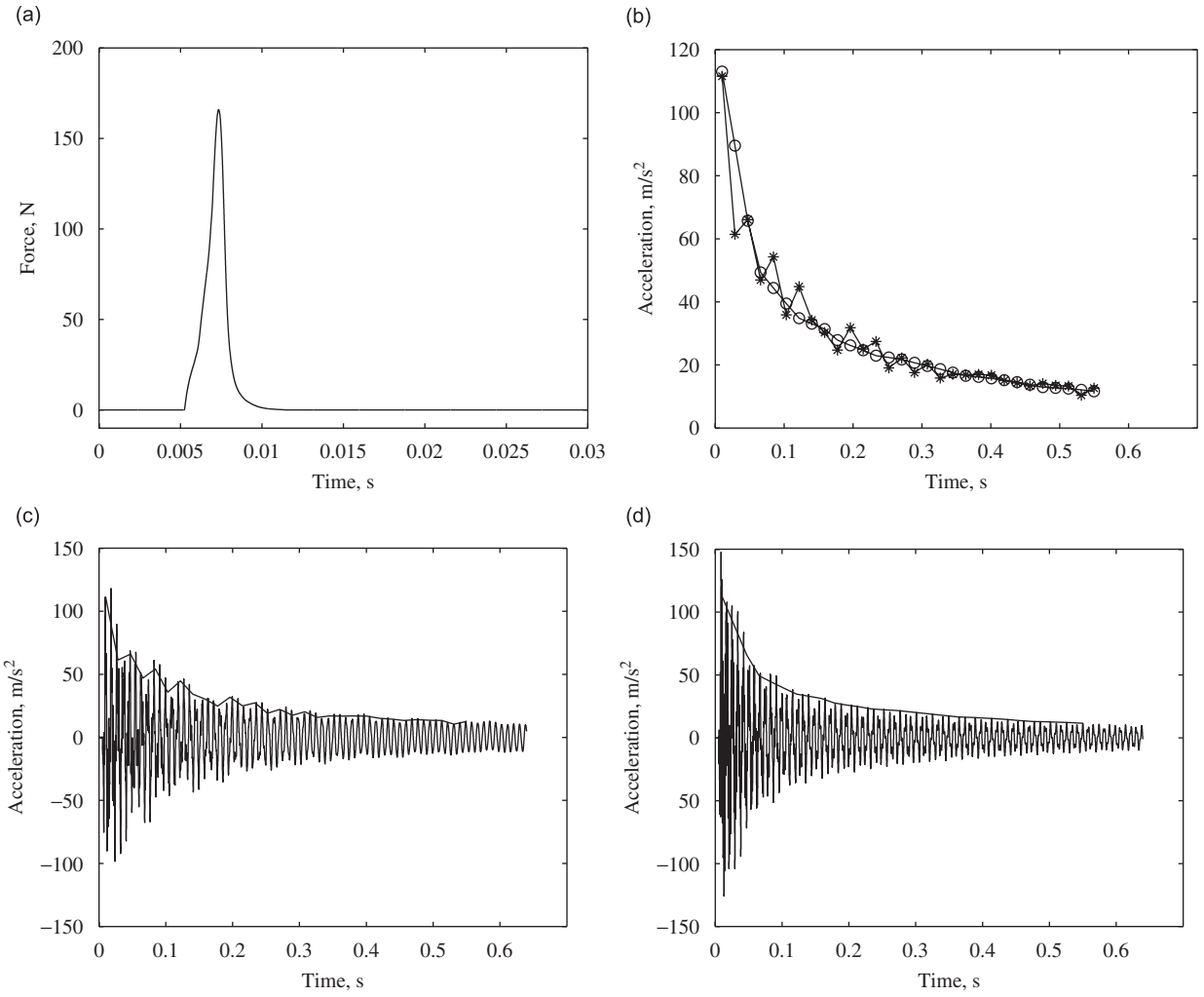

Fig. 8. Results for the validation case with 166 N impact: (a) forcing signal; (b) experimental and simulated envelopes, — ○ — measured, ... simulated; (c) measured response; (d) simulated response.

20 neurons. All neurons in the four hidden layers were defined to have the hyperbolic tangent sigmoid transfer function tansig [12], and the two output neurons (one outputs the slip force f_{yi}, and the other yields the stiffness ratio α) were defined to have the linear transfer function purelin [12] expressed as

$$\text{tansig}(x) = \frac{2}{1+e^{-2x}} - 1 \quad \text{and} \quad \text{purelin}(x) = x. \tag{5}$$

The network was trained using the error back-propagation algorithm. To ensure that the network does not over-fit the training data points and to evaluate the accuracy of the estimation procedure, a validation data set was produced using a similar procedure as described previously. Parameters for validation data set were chosen to be such that the slip force was varied from 90 to 210 N with increments of 20 N, and the stiffness ratio was varied from 0.12 to 0.27 with increments of 0.05. Fig. 12 contains the relative error surfaces for both training and validation data sets of the estimation procedure using the steady-state response data. Similarly, a validation data set was created for the estimation procedure using decay envelopes. The slip force was varied from 610 to 790 N with increments of 20 N, while the stiffness ratio was varied from 0.45 to 0.75 with increments of 0.1. Fig. 13 contains the error surfaces resulting from training and validation data sets for the identification procedure based on the decay envelopes. Note that the amount of error is roughly the same for

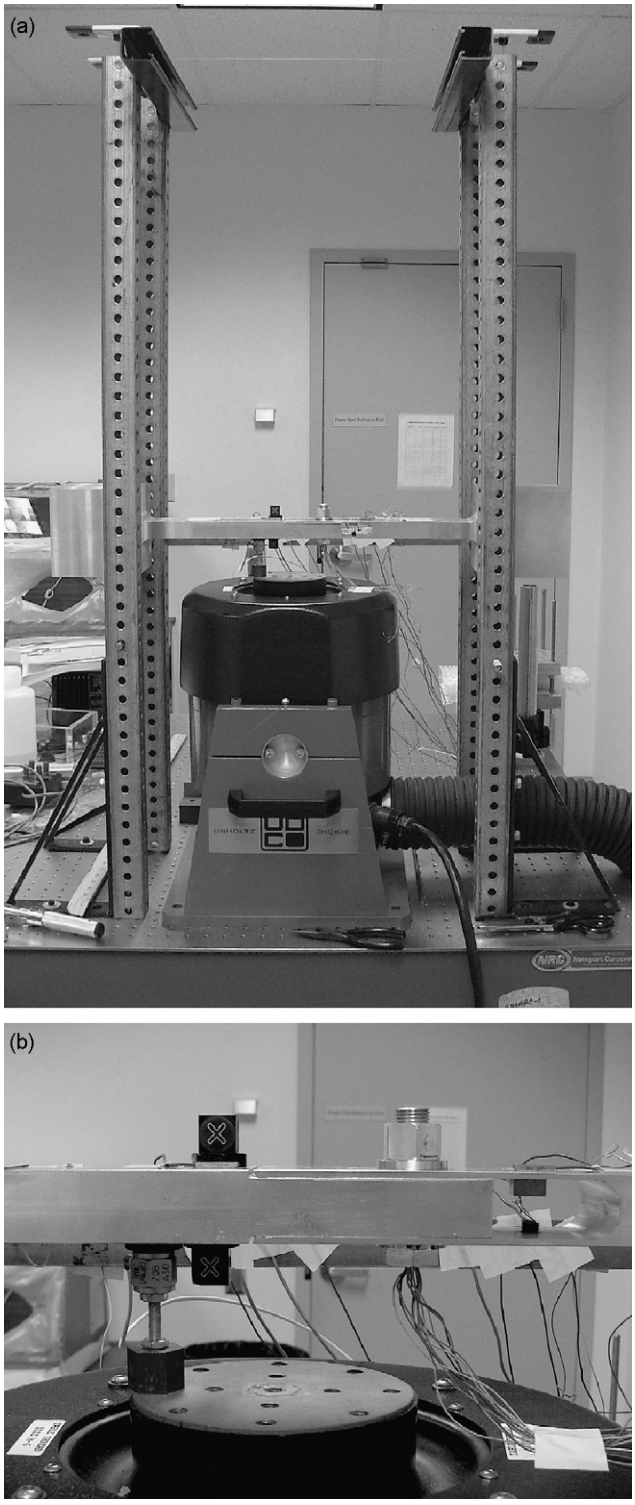

Fig. 9. Shaker attachment to the specimen: (a) general view of the experiment; (b) close-up view of the attachment.

the validation and training data sets. This shows that the neural networks do not over-fit the training data. From Figs. 12 and 13 one can conclude that the two parameter estimation techniques produce comparable relative errors in validation data, and hence their accuracy is roughly the same.

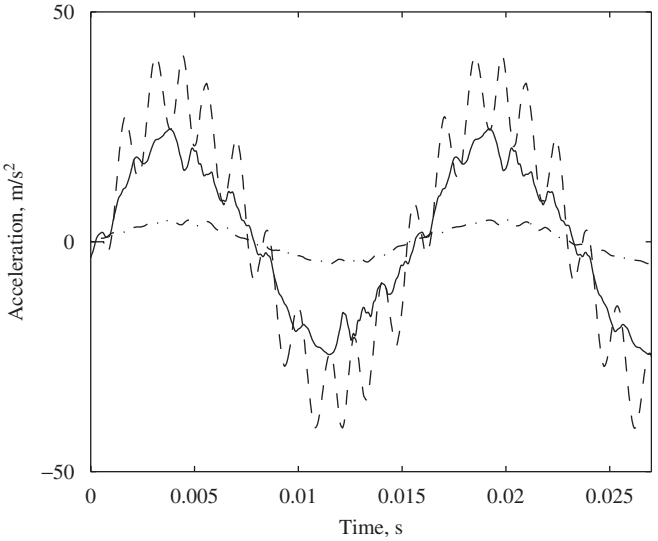

Fig. 10. Data obtained with AIB element parameters from high energy dissipation region, $f_{yi} \in \{80 \ldots 220\}$ and $\alpha \in \{0.1 \ldots 0.3\}$, - - - high dissipation, – · – · – low dissipation, —— experimental.

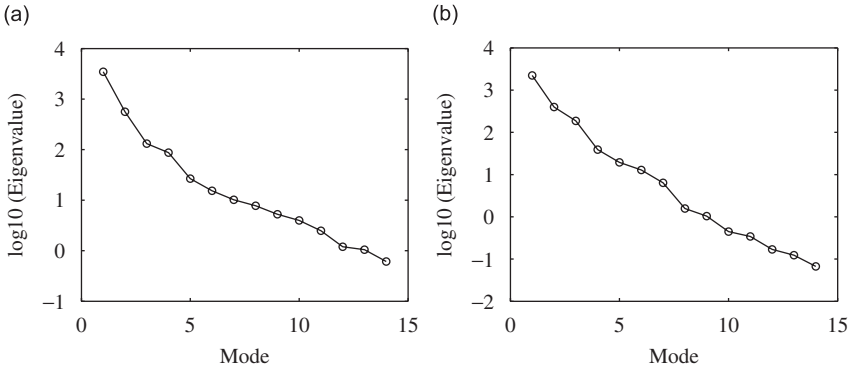

Fig. 11. Eigenvalues for principal component analysis: (a) acceleration data; (b) strain data.

Measured acceleration and strain data were processed using the same settings for wavelet transform and projected on the previously obtained principal components to obtain the input vector for the estimation procedure. The input vector was fed into the trained neural network yielding the following AIB element parameter values — $f_{yi} = 81.92$ and $\alpha = 0.1078$. The obtained values are close to the edge of the training parameter region, but no extrapolation has occurred. The response of the finite element model using the estimated parameters is shown in Fig. 14. From the time history plots, it is clear that the identified model is only able to replicate large-scale behavior of the system. That is, the higher frequency harmonics present in the measured data are not modeled very accurately and the measured data is overlapped by the prediction in the mean sense. A likely reason for this discrepancy is the AIB element with the previously mentioned parametric assumptions is not able to capture all of the complex dynamics that occur at the joint's interfaces. Note that in the case with decay envelopes, the AIB element was specifically intended to represent large-scale dynamics of the system, such as the initial amplitude and its decay rate; fine details were not captured.

Two important conclusions are supported by the results presented above: (1) the somewhat restrictive assumptions about the AIB element parameters should perhaps be relaxed to improve simulation quality and adaptability, and (2) two very different sets of AIB element parameters were needed to describe the system undergoing qualitatively different types of excitation.

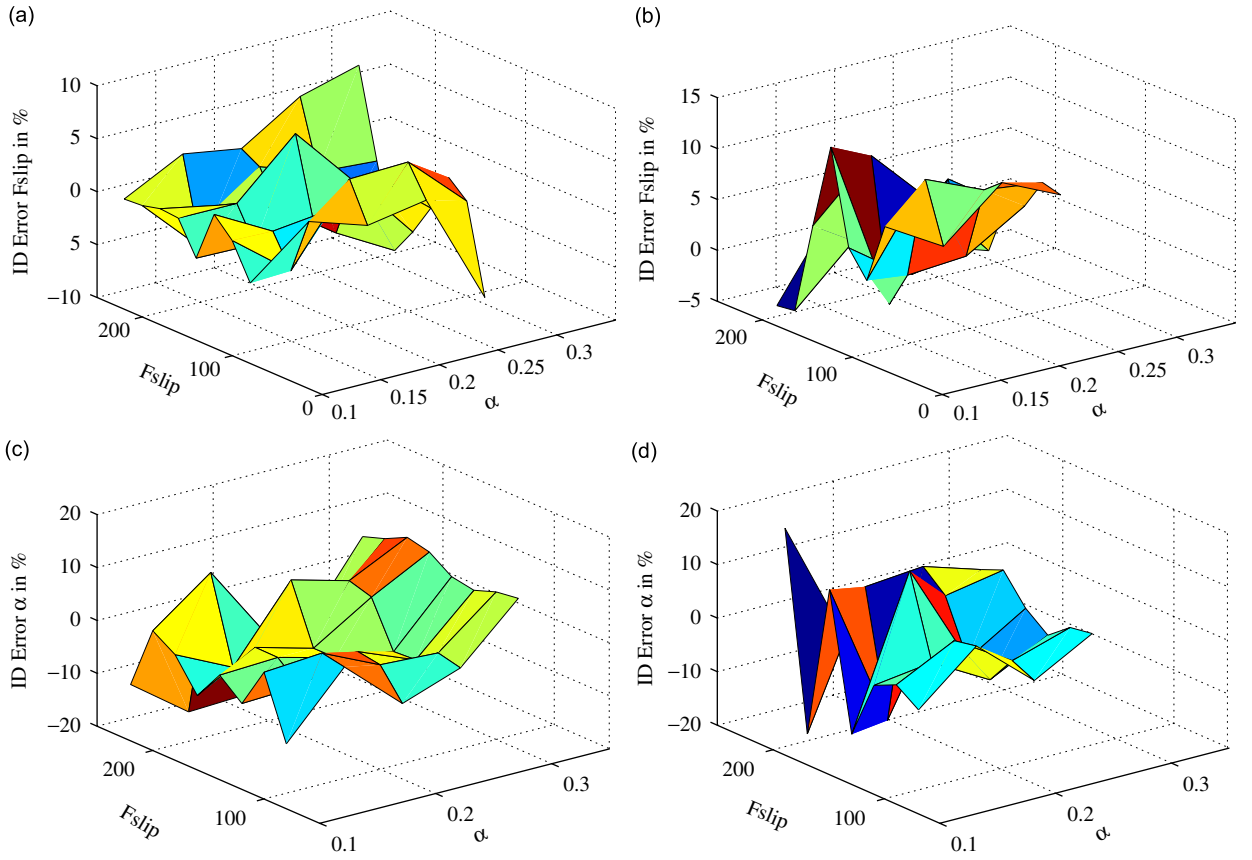

Fig. 12. Error surfaces for the estimated parameters for the procedure based on steady-state oscillatory response: (a) error in the estimated slip force for the training data set; (b) error in the estimated slip force for the validation data set; (c) error in the estimated stiffness ratio for the training data set; (d) error in the estimated stiffness ratio for the validation data set.

6. Summary and conclusions

The AIB element was applied to model the response of a joined structure to sustained sinusoidal input. Key assumptions were made to facilitate experimental estimation of the constitutive parameters; in particular, the two adjusted Iwan models that constitute the beam element used to model the joint, shared the same parameters. This assumption is similar that made by Song et al. [5] in previous work in order to simplify parameter estimation procedure. The results presented herein reveal that a unique set of model parameters does not allow representation of the dynamic behavior of the structure under varied types of excitation.

An alternative parameter estimation approach that utilizes steady-state oscillatory data was developed. The application of the new approach was demonstrated on the experimental data, but the model is only able to replicate the large-scale behavior of the system. The study performed here suggests that the accuracy of the proposed estimation technique is comparable to that of the method utilizing decay envelope data for parameter estimation. A necessary future step in the development of this joint model is to attempt to quantify variability of the joints by identifying common ranges of Iwan parameters. In addition, ability of the AIB element to model responses from different excitation magnitudes needs to be investigated. In order to allow for eventual use of this model in a risk-based design the accuracy of parameter estimation also should be improved.

More research needs to be done to investigate the performance of the AIB element when key assumptions made in this work are relaxed. More specifically, the two adjusted Iwan models could have different slip forces and stiffness ratios, as well as possess non-uniform distribution functions for the sliders. However, the task of parameter estimation in these cases may become significantly more complicated, owing to the larger number

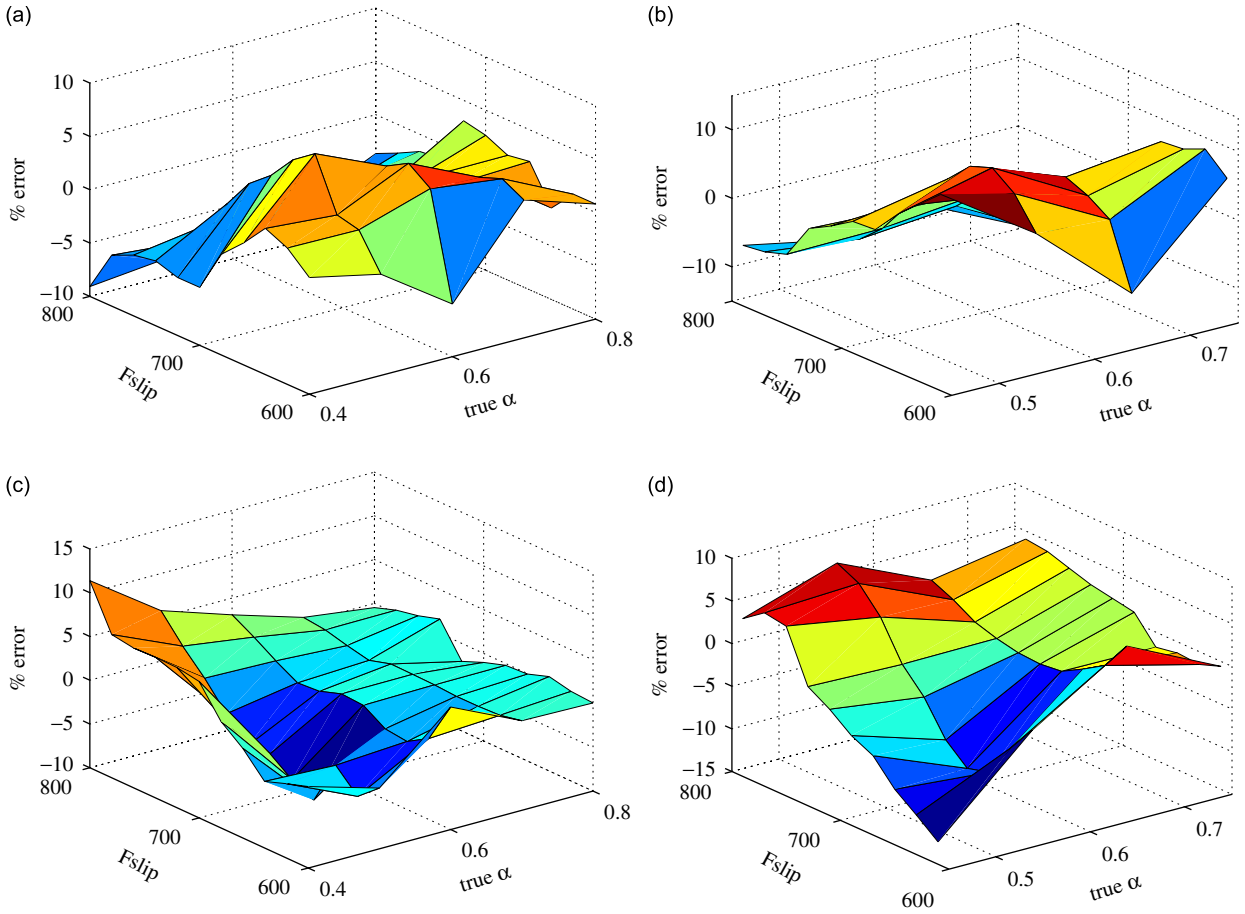

Fig. 13. Error surfaces for the estimated parameters for the procedure based on decay envelopes: (a) error in the estimated slip force for the training data set; (b) error in the estimated slip force for the validation data set; (c) error in the estimated stiffness ratio for the training data set; (d) error in the estimated stiffness ratio for the validation data set.

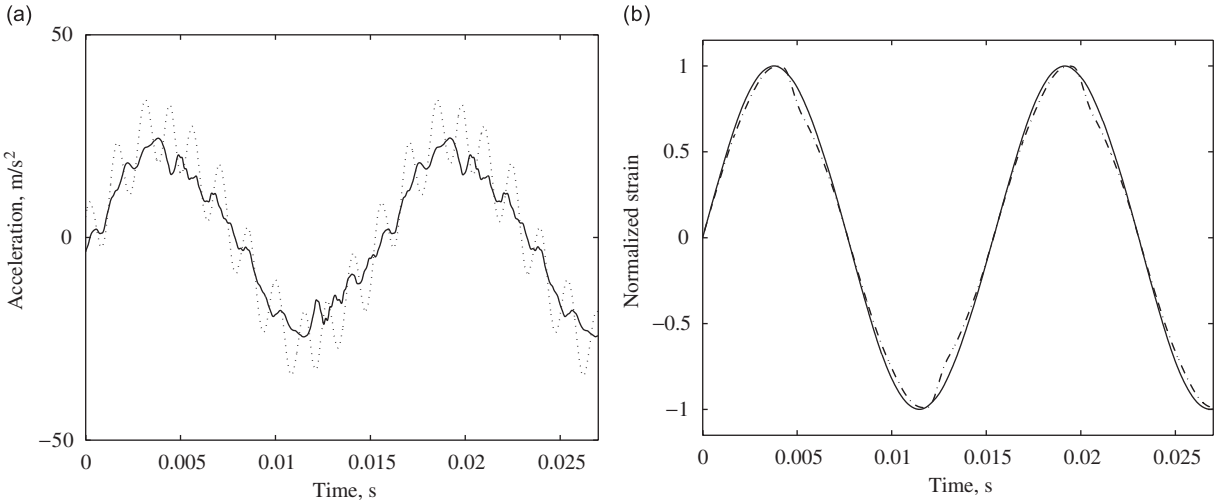

Fig. 14. Comparison of measured and simulated responses: (a) acceleration data. —— Experimental, ... numerical; (b) strain data. —— Experimental, ·— · —· numerical.

of parameters that must be estimated and possible similarities of the response features for different realizations of model parameters.

Acknowledgments

This work was done under AFRL/VA contract F33615-98-D-3210. Additional support was provided by the Dayton Area Graduate Studies Institute (DAGSI) and Wright State University Graduate Council Scholar Fellowship. The authors would also like to acknowledge Dr. Nathan Klingbeil and Dr. Jeremy Daily for provision of computational resources, as well as Mr. Greg Wilt and Mr. Jonathan Smith for their efforts on the experimental part in this project.

References

[1] R.A. Ibrahim, C.L. Pettit, Uncertainties and dynamic problems of bolted joints and other fasteners, *Journal of Sound and Vibration* 279 (2005) 857–936.
[2] X. Yue, Development of Joint Elements and Solution Algorithms for Dynamic Analysis of Jointed Structures, PhD Thesis, University of Colorado at Boulder, 2002.
[3] C.L. Pettit, J.C. Slater, S.M. Page, O.V. Shiryayev, Measurements and modeling of variability in the dynamics of a bolted joint, *45th AIAA/ASME/ASCE/ASC/AHS Structures, Structural Dynamics & Materials Conference*, Palm Sprins, CA, April 19–22, 2004.
[4] D.J. Segalman, A four-parameter iwan model for lap-type joints, Technical Report SAND-2002-3828, Sandia National Laboratories, November 2002.
[5] Y. Song, C.J. Hartwigsen, D.M. McFarland, A.F. Vakakis, L.A. Bergman, Simulation of dynamics of beam structures with bolted joints using adjusted iwan beam elements, *Journal of Sound and Vibration* 273 (1–2) (2004) 249–276.
[6] W.D. Iwan, A distributed-element model for hysteresis and its steady-state dynamic response, *Journal of Applied Mechanics* 33 (1966) 893–900.
[7] W.D. Iwan, On a class of models for the yielding behavior of continuous and composite systems, *Journal of Applied Mechanics* 34 (1967) 612–617.
[8] C. Hartwigsen, Y. Song, D. McFarland, L. Bergman, A. Vakakis, Experimental study of nonlinear effects in a typical shear lap joint configuration, *Journal of Sound and Vibration* 277 (2004) 327–351.
[9] Hibbitt, Karlsson & Sorensen, Inc., RI *ABAQUS/Standard User's Manual*, Version 6.3, 2002. ⟨URL http://www.abaqus.com⟩.
[10] The MathWorks Inc., Natick, MA, Using MATLAB, July 2002.
[11] R. Cook, D. Malkus, M. Plesha, *Concepts and Applications of Finite Element Analysis*, third ed., Wiley, New York, 1989.
[12] H. Demuth, M. Beal, *Neural Network Toolbox User's Guide*, The MathWorks, Inc., Natick, MA, January 2003. ⟨URL http://www.mathworks.com⟩.
[13] M. Misiti, Y. Misiti, G. Oppenheim, J.-M. Poggi, *Wavelet Toolbox User's Guide*, The Mathworks, Inc., Natick, MA, second ed., July 2002.